Microwave Near-Field Probes for Photovoltaic Applications

Joel C. Weber[1,2], Kris A. Bertness[1], John B. Schlager[1], Norman A. Sanford[1], Atif Imtiaz[1], Thomas M. Wallis[1], Pavel Kabos[1], Kevin J. Coakley[1], Victor M. Bright[2], and Lorelle M. Mansfield[3]
[1]NIST, Boulder, CO, USA
[2]University of Colorado at Boulder, Boulder, CO, USA
[3]NREL, Golden, CO, USA

ABSTRACT

The photoresponse of three different photovoltaic Cu(In,Ga)Se_2 (CIGS) samples as well as GaAs and silicon bulk samples is measured using near-field scanning microwave microscopy (NSMM). Modeling predicts light-dependent conductivity values for bulk samples, as well as a preliminary understanding of more complicated multilayer photovoltaics. The spectral dependence of CIGS samples is probed at 405, 635, 808 and 980 nm wavelengths. In addition, we present two-dimensional raster scans that may reveal grain-boundary effects under illumination.

INTRODUCTION

We have used NSMM to probe the photoresponse of CIGS photovoltaic test structures and GaAs and silicon bulk samples subjected to optical excitation. NSMM can distinguish between bulk material properties [1] with nanometer-scale lateral spatial resolution in semiconductors at microwave frequencies [2]. This makes NSMM a valuable metrology tool for the study of photovoltaic material properties. In particular, NSMM probes properties that strongly influence transport and recombination of carriers, including grain boundaries, interfaces, defects, and compositional variations on a nanometer scale.

Our NSMM system is based on a scanning tunneling microscope (STM) layout with a DC feedback control that allows non-destructive sample characterization. The STM tip is coupled to a coaxial reflection microwave cavity with a resonance frequency near 4.5 GHz. Excess photogenerated carriers in the vicinity of the probe tip alter the load on the cavity, thereby shifting the resonance frequency. Under continuous- wave optical illumination at a series of different wavelengths, CIGS, GaAs and silicon samples yielded measurable shifts in resonant frequency of the cavity. In addition, raster scan images reveal spatial features related to optical excitations that are on the order of the expected grain size (.5 to 1 μm) in CIGS samples.

EXPERIMENTAL SETUP

A detailed description of the NSMM, which was designed and assembled at NIST, has been previously published [3]. While the microwave circuit and STM feedback mechanism remain unchanged, several improvements have been made that expand the tool's capabilities and reduce measurement error. The z-axis positioning system was refitted to allow for sample movement while holding the tip stationary. Previous measurements indicated that tip movement over distances as small as several micrometers mechanically disrupted the microwave circuit. This significantly altered the Q of the resonance curve and limited modeling effectiveness. A new closed-loop system enables precise, reproducible sample control at ~2 nm without affecting the microwave circuit.

The primary illumination source is a diffuse, blue diode laser operating at a wavelength of 405 nm with an approximate intensity at the tip/sample interface of 0.160 W/cm^2. Additional highly focused diode laser sources at 405, 635, 808, and 980 nm enable characterization of individual PV samples across the spectral range. The power source and optical specifications were used to calculate approximate spot diameters and average uniform intensities, as summarized in Table 1.

	405 nm	635 nm	808 nm	980 nm
Spot diam. (cm)	0.006	0.002	0.002	0.004
Intensity (W/cm^2)	200	600	1000	400

Table 1 Relative spot diameters and intensity values for various lasing wavelengths.

A detailed view of the sample stage, lasing source and microwave-enabled tip is shown in Fig. 1.

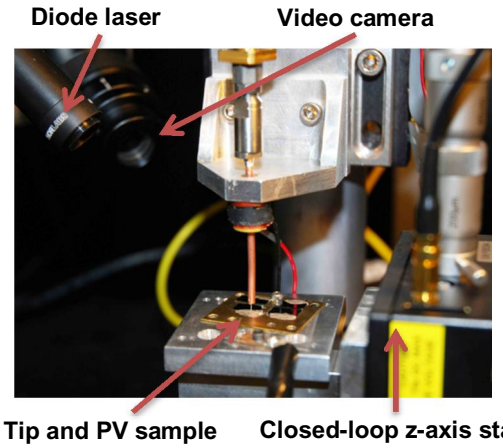

Figure 1 Image of NSMM probe highlighting the sample stage and light source.

The photovoltaic samples used in this study consisted of three different CIGS samples, designated CS30, CS70 and CS99 [3-9]. Their respective Ga mole fractions were varied during fabrication, resulting in average efficiency ratings of 3.8 %, 12.8 % and 16.8 %, respectively. Material properties of CIGS samples are outlined in Table 2 below.

Sample	Ga mole fraction	Run #	CIGS thickness (μm)	Avg. Efficiency (%)
CS30	0.3	C2554	2.0	16.8
CS70	0.7	C2553	1.8	12.8
CS99	0.99	C2525	2.1	3.8

Table 2 CIGS sample properties and measured efficiencies.

In addition to the PV samples tested, bulk GaAs (500 μm thick) and silicon samples were also acquired in order to aid in model development. Known parameters are reported in Table 3. Curve-fitting based on experimental data will be presented in the following section.

Sample	Doping (cm^{-3})	Mobility (cm^2/V-s)	Resistivity (Ω-cm)
GaAs	3-4 E7	7000	2.1-3.3 E7
Silicon	-	-	1-20

Table 3 Bulk GaAs and silicon sample parameters.

RESULTS AND DISCUSSION

Modeling of Height Scans

We collect data for modeling by tracking frequency shifts as a function of tip/sample distance. These shifts can then be fitted in order to determine the change in carrier concentration under illumination. The tip is initially brought to within ~10 nm of the sample while under illumination from the diffuse 405 nm laser diode. The sample is then retracted, while the tip is held stationary, over a distance of 3 μm. This process is repeated but with the light source turned off prior to retracting the sample. The tip/sample interaction can be modeled as a resistance-inductance-capacitance (RLC) circuit with shifts in the resonant frequency corresponding to capacitance changes [10]. As is illustrated in Fig. 2, the circuit consists of three separate capacitances in series: coupling capacitance between the tip and the sample ($C_{coupling}$), depletion layer capacitance ($C_{depletion\_layer}$) and bulk sample capacitance (C_{bulk}).

Frequency shifts were determined from the measurements by use of a resonance model [11]. For GaAs (Fig. 3(a)), a greater frequency shift is found in the illuminated state, indicating a higher conductivity. The model requires a ~2% increase in carrier concentration to account for the greater frequency drop, comparable to reported values [12]. Deviations between the fit and the experimental data are due to the large skin depth of the GaAs sample. Microwaves were able to penetrate to the copper sample holder and subsequently altered bulk properties.

When the silicon sample is illuminated, a large frequency shift is observed (Fig. 3(b)). Here, the higher conductivity in the illuminated state results in a large complex permittivity value. This leads to the change in concavity between the dark and illuminated experimental data, with the illuminated state exhibiting a concave downwards trend. The model requires a ~500 % increase in carrier concentration, which is feasible for a silicon sample [13].

A copper plate served as a control for our height dependence measurements. As a conductor, the conductivity of copper is insensitive to light. Thus, any measured changes between the dark and illuminated state can likely be attributed to temperature affects from the laser diode heating the tip and sample. Figure 3(c) illustrates that the differences in dark and illuminated data are negligible, indicating that temperature effects play no significant role.

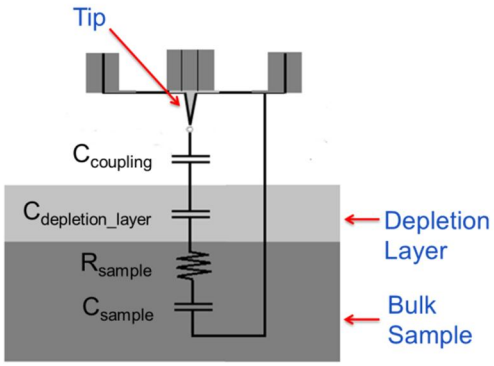

Figure 2 RLC model of tip/sample interaction comprised of three separate capcitances in series.

Spectral Dependence of CIGS Samples

We quantified the spectral response of CS30 and CS70 CIGS samples by use of continuous-wavelength optical illumination at each of four wavelengths. To eliminate height dependent effects, the NSMM tip was brought into contact with the sample under illumination at the wavelength in question. The resonance frequency was recorded prior to turning off the light source. At this point, the frequency shift due to the change in charge carriers was also recorded. This experiment was conducted five times at each wavelength on each sample to provide the data points and respective standard deviations shown in Fig. 4(a). It can be seen that the more efficient CS30 sample has a statistically significant greater frequency shift at all wavelengths except for 635 nm. As shown earlier in Table 1, the spot diameters and subsequent intensities at each wavelength vary. However, this can be accounted for by comparing the difference in frequency shifts between CS30 and CS70 at each wavelength with the difference in spectral-dependent quantum efficiency values (Fig. 4(b)) [14] as is shown in Fig. 4(c). The frequency and quantum efficiency differences are plotted on separate axes and have their maximum values normalized to one another. Here, the respective

differences follow roughly similar trends, indicating that the two measurements track each other relatively well. The exception occurs at 405 nm, where a much greater than expected frequency shift is found. This occurs because the quantum efficiency data was recorded with the top passivation layer intact. This layer absorbs wavelengths shorter than 490 nm and thus the actual quantum efficiency response for unpassivated samples is unknown.

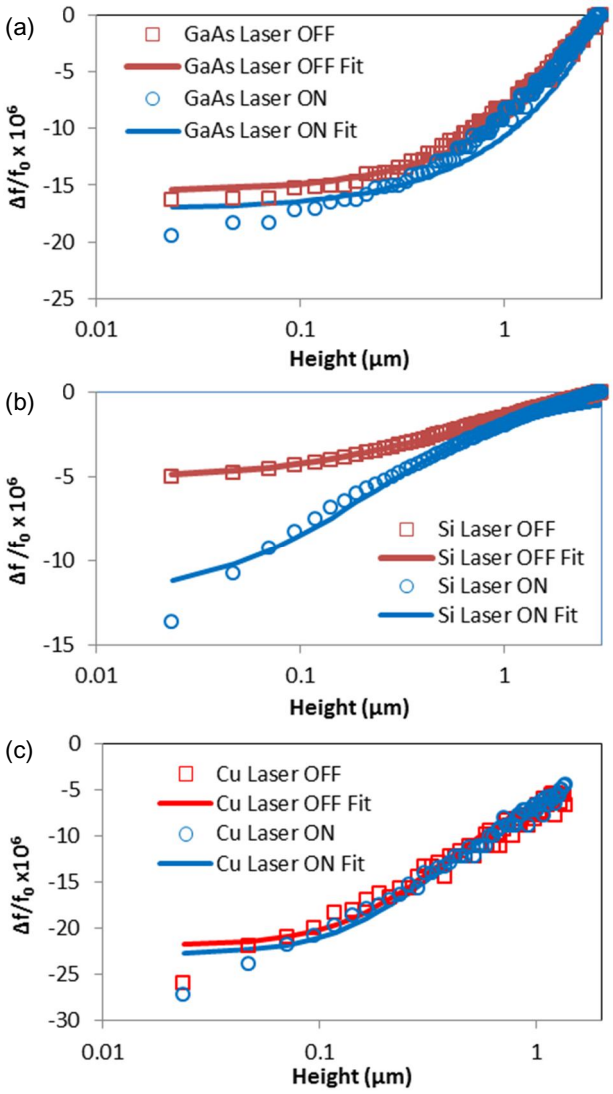

Figure 3(a) GaAs height-dependent frequency shifts fitted with model for dark and illuminated states. Large skin depth at low conductivities enables microwaves to penetrate to the metal sample stage. This is accounted for by shifting the entire fitted curve vertically.
Figure 3(b) Silicon height-dependent frequency shifts fitted with model for dark and illuminated states.
Figure 3(c) Copper height-dependent frequency shifts fitted with model for dark and illuminated states. Overlapping data indicates negligible temperature effects from laser diode.

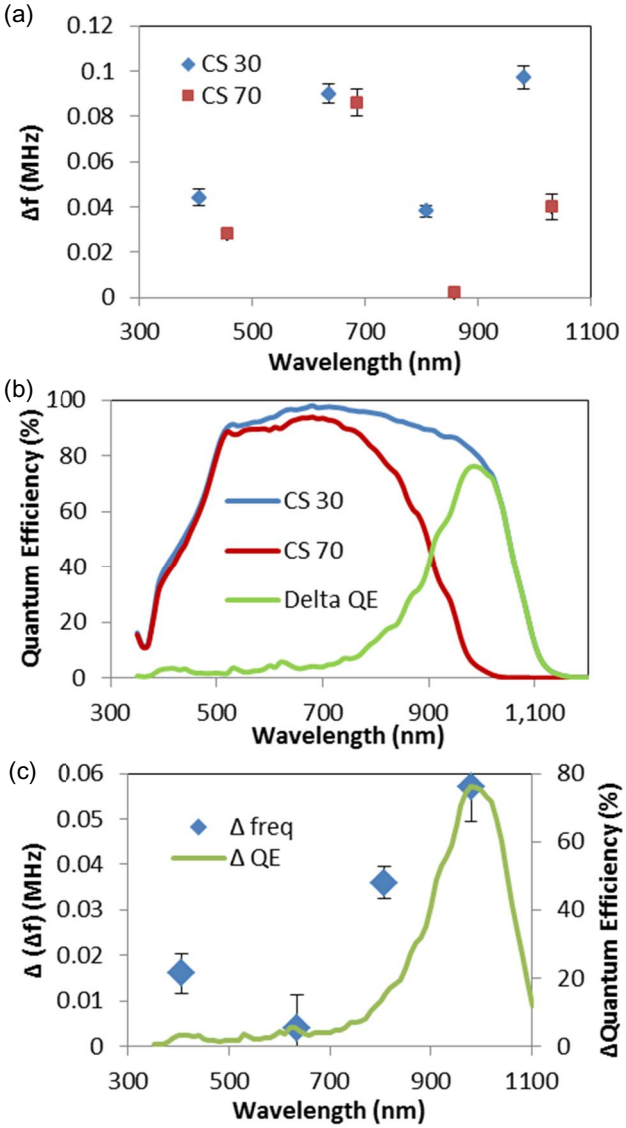

Figure 4(a) Frequency shifts for CS30 and CS70 at 405 nm, 635 nm, 808 nm and 980 nm. For viewing clarity, CS70 data has been shifted 50 nm along the x-axis.
Figure 4(b) Spectral dependence of the quantum efficiency for CS30 (blue), CS70 (red) and the difference between the two (green) [13].
Figure 4(c) Difference in frequency shifts plotted against difference in quantum efficiency as a function of wavelength.

2D Scanning and Analysis

Raster scans encompassing a 1 μm x 1 μm portion of CS99 in dark and illuminated states have been reported with an average shift in S_{11} of over 7 dB [3]. Images were acquired by measuring the change in S11 as a function of lateral tip position, with and without illumination of a blue diode laser. The large shifts seen are similar to those previously modeled for a silicon solar cell [15]. To avoid inducing height variations into the STM feedback system

caused by changes in conductivity across the sample, active feedback was suspended for these scans and the tip was placed ~10 nm outside of contact with the sample. As can be seen in Fig. 5(a), this resulted in a noticeable tip drift and sample tilt viewable in the dark condition. In addition to a large shift in measured microwave power, the illuminated scan in Fig. 5(b) also yields features spaced apart on the order of 0.5 μm, comparable to the measured CS99 grain size.

We developed a method to better reveal significant features in NSMM images. For both the dark state and the illuminated state of the photovoltaic device, magnitude (of the S_{11}) images were formed. The dark state magnitude image was then subtracted from the illuminated state magnitude image to get a difference image. We estimate a smoothly varying trend in this difference image (attributable to tip drift and sample tilt) with a robust local smoothing method [16]. This trend is subtracted from the difference image to get a residual image. This residual image is then denoised with the Adaptive Weights Smoothing (AWS) method resulting in Fig. 5(c) [17]. In the AWS method, a local likelihood model is fit to a neighborhood centered on each pixel. The AWS method adaptively determines the size and associated weights for each local neighborhood. This allows us to simultaneously remove additive noise while preserving edge features. The denoised image produced by the AWS method reveals a clearly defined vertical region across the scan, which may indicate potential charge trapping at a grain boundary in the CS99 sample. Current implementation of a tuning fork based feedback system will enable confirmation of this initial result by overlaying topographical information with microwave data.

SUMMARY

We have demonstrated NSMM sensitivity to photovoltaic and bulk semiconductor samples across several different illumination wavelengths. Bulk GaAs and silicon height scan data were fit using an RLC model, laying the foundation for the development of a more advanced multilayer photovoltaic model. NSMM spectral response measurements between CIGS samples showed comparable qualitative trends between frequency and quantum efficiency differences. Finally, analysis of 2D scans taken on CIGS in dark and illuminated states provided evidence for charge trapping at grain boundaries. Further modification to the NSMM through the addition of a tuning fork feedback system should enable a topographical overlay and subsequent verification of this result.

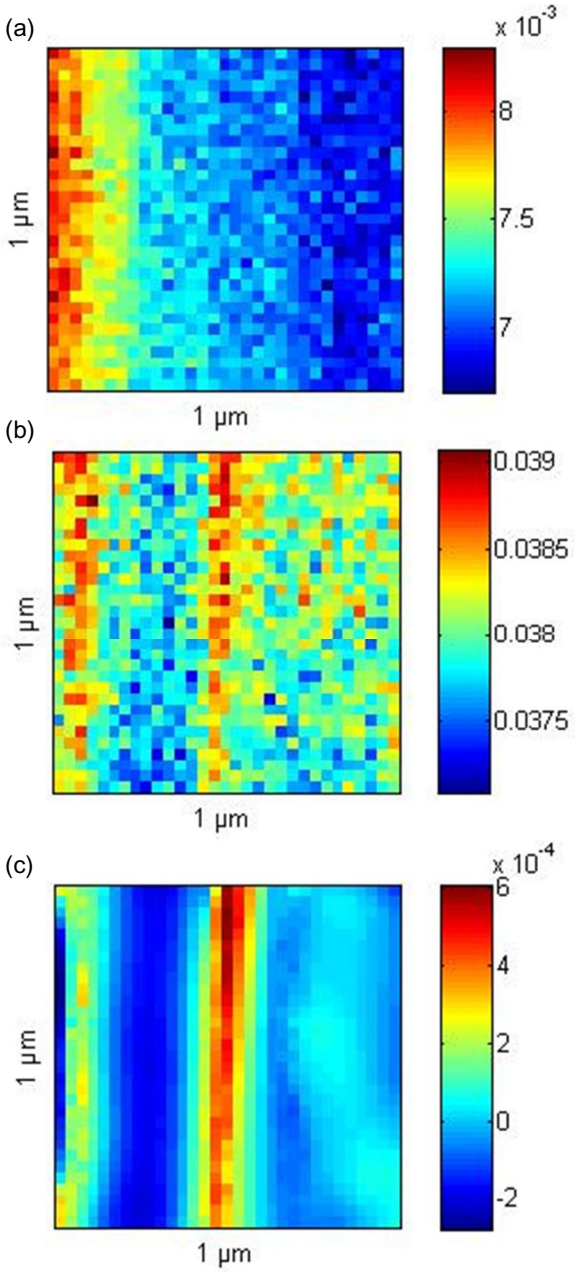

Figure 5(a) Scan of CS99 with laser off showing drift in tip/sample distance.
Figure 5(b) Scan of CS99 under illumination with appearance of grain-sized features.
Figure 5(c) Difference between dark and illuminated scans with trend removed and the image denoised. Potential charge trapping along grain boundary becomes apparent.
For all three figures, color scale values are reported as power magnitudes with respect to a 10 W source.

ACKNOWLEDGEMENTS

The studies conducted by the authors from the University of Colorado-Boulder are supported by the DARPA Center on Nanoscale Science and Technology for Integrated Micro/Nano-Electromechanical Transducers (iMINT), supported (in part, if applicable) by the Defense Advanced Research Projects Agency (DARPA) N/MEMS S&T Fundamentals program under grant no. N66001-10-1-4007 issued by the Space and Naval Warfare Systems Center Pacific (SPAWAR).

Aric Sanders and Tasshi Dennis provided critical reading of the manuscript.

REFERENCES

[1] A. Imtiaz, T. Baldwin, H. T. Nembach, T. M. Wallis, and P. Kabos, "Near-field microwave microscope measurements to characterize bulk material properties," *Appl. Phys. Lett.,* **90**, p. 243105, (2007).

[2] A. Imtiaz, S. M. Anlage, J. D. Barry and J. Melngailis, "Nanometer-scale material contrast imaging with a near-field microwave microscope", *Appl. Phys. Lett.,* **90**, p. 143106, (2007).

[3] K. Bertness, J. Schlager, N. Sanford, A. Imtiaz, T. Wallis, J. Weber, P. Kabos and L. Mansfield, "Application of microwave scanning probes to photovoltaic material," *PVSC, 2010 35th IEEE*, p. 001669-001674, (2010)

[4] U. S. Patent No. 5,441,897 (August 15, 1995).

[5] U. S. Patent No. 5,436,204 (July 25, 1995).

[6] M. A. Contreras, B. Egaas, K. Ramanathan, J. Hiltner, A. Swartzlander, F. Hasoon, and R. Noufi, "Progress toward 20% efficiency in Cu(In,Ga)Se2 polycrystalline thin-film solar cells," *Progress in Photovoltaics: Research and Applications,* vol. 7, pp. 311-316, 1999.

[7] M. A. Contreras, J. Tuttle, A. Gabor, A. Tennant, K. Ramanathan, S. Asher, A. Franz, J. Keane, L. Wang, J. Scofield, and R. Noufi, "High efficiency Cu(In,Ga)Se_2-based solar cells: processing of novel absorber structures," in *Conference Record of the Twenty Fourth. IEEE Photovoltaic Specialists Conference - 1994*, 1994, pp. 68-75.

[8] K. Ramanathan, M. A. Contreras, C. L. Perkins, S. Asher, F. S. Hasoon, J. Keane, D. Young, M. Romero, W. Metzger, R. Noufi, J. Ward, and A. Duda, "Properties of 19.2% efficiency ZnO/CdS/CuInGaSe2 thin-film solar cells," *Progress in Photovoltaics,* vol. 11, pp. 225-230, 2003.

[9] M. A. Contreras, M. J. Romero, B. T. E. Hasoon, R. Noufi, S. Ward, and K. Ramanathan, "Optimization of CBD CdS process in high-efficiency Cu(In,Ga)Se-2-based solar cells," *Thin Solid Films,* vol. 403, pp. 204-211, 2002.

[10] M. Tabib-Azar, D.-P. Su, A. Pohar, S. R. LeClair, and G. Ponchak, "0.4 mm spatial resolution with 1 GHz (l =30 cm) evanescent microwave probe," *Rev. Scientific Instruments,* vol. 70, pp. 1725-1729, 1999.

[11] C. Gao and X.-D. Xiang, *Review of Scientific Instruments,* vol. 69, p. 3846, 1998.

[12] H. Kunzel, G. H. Dohler and K. Ploog, "Determination of photoexcited carrier concentration and mobility in GaAs doping superlattices by Hall effect measurements," *Appl. Phys. A*, **27**, p. 1, (1982).

[13] L. S. Yu, Q. Z. Liu, Z. F. Guan and S. S. Lau, "Direct measurement of the refractive index change of silicon with optically injected carriers," *Appl. Phys. Lett.*, **68**, p. 1546, (1996).

[14] Data for figure provided by NREL.

[15] A. Hovsepyan, A. Babajanyan, T. Sargsyan, H. Melikyan, S. Kim, J. Kim, K. Lee, and B. Friedman, "Direct imaging of photoconductivity of solar cells by using a near-field scanning microwave microprobe," *Journal of Applied Physics,* vol. 106, p. 114901, 2009.

[16] C. Loader, "Local regression and likelihood," *Springer*, New York, (1999).

[17] J. Plzehl and V. Spokoiny, "Propagation-separation approach for local likelihood estimation," *Prob. Theory and Rel. Fields,* **135**, p. 335, (2006).